AD–A110 786   THAYER SCHOOL OF ENGINEERING HANOVER N H   F/G 20/11
                FACTORS INFLUENCING THERMOMECHANICAL FAILURE OF FACE SEALS.(U)
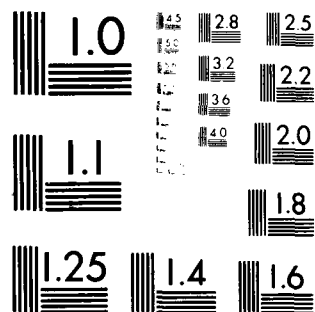   JAN 82   F E KENNEDY, J N GRIM, R P GLOVSKY   N00014-81-K-0090
UNCLASSIFIED   NL

END
DATE
FILMED
3-82
DTIC

1.0

4.5
5.0

2.8

2.5

3.2

2.2

3.6

1.1

4.0

2.0

1.8

1.25

1.4

1.6

MICROCOPY RESOLUTION TEST CHART

NATIONAL BUREAU OF STANDARDS 1963 A

LEVEL II

(12)

FACTORS INFLUENCING
THERMOMECHANICAL FAILURE OF FACE SEALS

by

Francis E. Kennedy, Jr., John N. Grim and Roger P. Glovsky

Interim Report
submitted to

January, 1982

8 202 10 085

THAYER
SCHOOL
OF
ENGINEERING

1867

AN ASSOCIATED SCHOOL OF DARTMOUTH COLLEGE, HANOVER, NEW HAMPSHIRE

Unclassified

REPORT DOCUMENTATION PAGE		READ INSTRUCTIONS BEFORE COMPLETING FORM
1. REPORT NUMBER	2. GOVT ACCESSION NO.	3. RECIPIENT'S CATALOG NUMBER
4. TITLE (and Subtitle) FACTORS INFLUENCING THERMOMECHANICAL FAILURE OF FACE SEALS		5. TYPE OF REPORT & PERIOD COVERED Interim Report Dec 1, 1980-Nov. 30, 1981
		6. PERFORMING ORG. REPORT NUMBER
7. AUTHOR(s) Francis E. Kennedy, Jr. John N. Grim Roger P. Glovsky		8. CONTRACT OR GRANT NUMBER(s) N00014-81-K-0090
9. PERFORMING ORGANIZATION NAME AND ADDRESS Thayer School of Engineering Dartmouth College Hanover, NH 03755		10. PROGRAM ELEMENT, PROJECT, TASK AREA & WORK UNIT NUMBERS
11. CONTROLLING OFFICE NAME AND ADDRESS Engineering Science Directorate Office of Naval Research Arlington, Va. 22217		12. REPORT DATE January 1982
		13. NUMBER OF PAGES 55
14. MONITORING AGENCY NAME & ADDRESS(if different from Controlling Office)		15. SECURITY CLASS. (of this report) Unclassified
		15a. DECLASSIFICATION/DOWNGRADING SCHEDULE

16. DISTRIBUTION STATEMENT (of this Report)

Approved for public release; distribution unlimited.

17. DISTRIBUTION STATEMENT (of the abstract entered in Block 20, if different from Report)

18. SUPPLEMENTARY NOTES

19. KEY WORDS (Continue on reverse side if necessary and identify by block number)

Mechanical Seals, Face Seals, Seals, Thermal Stress, Thermoelastic, Failure, Cracks.

20. ABSTRACT (Continue on reverse side if necessary and identify by block number)

A microscopic examination, an analytical study, and an experimental study were carried out to determine why and how thermocracking occurs in the mating ring of a mechanical face seal. Microscopic examination of the cobalt-based superalloy mating ring of a marine propeller shaftseal yielded a better understanding of the initiation and propagation of thermocracks in the seal ring and of the role played by second phase particles in thermocracking. An analysis of surface temperatures and stresses in the

DD FORM 1473 EDITION OF 1 NOV 65 IS OBSOLETE
1 JAN 73
S/N 0102-LF-014-6601

Unclassified

seal, using finite element techniques, showed that the dominant stresses in the seal components are thermal stresses. A thermocracking mechanism is proposed, based on the analytical study, which agrees well with all microscopic features. The analytical model assumed that thermoelastic instabilities cause concentrated contact patches to form at the seal interface prior to the onset of thermocracking. The presence of these contact patches was confirmed by use of a novel contact probe in the experimental study. Suggestions are made of steps that could be taken to alleviate the thermocracking problem and guidance is offered for the choice of future seal materials.

FACTORS INFLUENCING
THERMOMECHANICAL FAILURE OF FACE SEALS

Interim Report
submitted to

by

Francis E. Kennedy, Jr.
Associate Professor of Engineering

and

John N. Grim and Roger P. Glovsky
Graduate Research Assistants

Thayer School of Engineering
Dartmouth College
Hanover, N.H. 03755

January, 1982

FOREWORD

TABLE OF CONTENTS

LIST OF FIGURES

LIST OF TABLES

INTRODUCTION AND BACKGROUND

Introduction

Mechanical face seals are widely used to prevent the leakage of a fluid along a rotating shaft which passes through a stationary housing or pressure vessel. Many different mechanical face seal configurations are possible (see, for example, Ref. 1), but all feature a sealing surface which lies normal to the axis of the shaft and which consists of a flat rotating ring in contact with a flat stationary ring. One such seal is the primary shaft seal used in ships and submarines to prevent intrusion of sea water along the rotating propeller shaft. An example of a marine propeller shaft seal is shown in Figure 1. In that particular seal, a mating ring made from a cobalt-based superalloy is attached to the rotating shaft. Its flat face rubs against the ground nose of a non-rotating primary sealing ring made from carbon-graphite. The seal is externally pressurized by sea water. A typical shaft seal of this type could have a diameter of 50 cm or more and could operate at a PV value (= sealed fluid pressure x sliding velocity of seal face) of over 10 $MNs^{-1}m^{-1}$. The seal typically has a pressure balance of between 70 and 75%.

Mechanical face seals have proven to be the most effective means of providing rotary shaft sealing in many severe applications such as the one described. As the severity of the application increases, however, the frequency of seal failure, as indicated by excessive leakage and/or excessive friction, also increases (1). In the newer submarines, for example, many early failures of the large, heavily-loaded primary shaft seals have been encountered. Since such failures can lead to a delay in or curtailment of the vessel's mission, it is necessary that seal failures be avoided, if possible. Upon disassembly of a seal after such a failure it is frequently found that the surface of the metallic mating ring contains numerous cracks. These cracks, called thermocracks or heat checks, contribute to excessive wear of the primary ring, warping of the mating ring, excessive seal leakage, and, occasionally, fracture of the mating ring. The shaft seal shown in Figure 1 has not escaped thermocracking
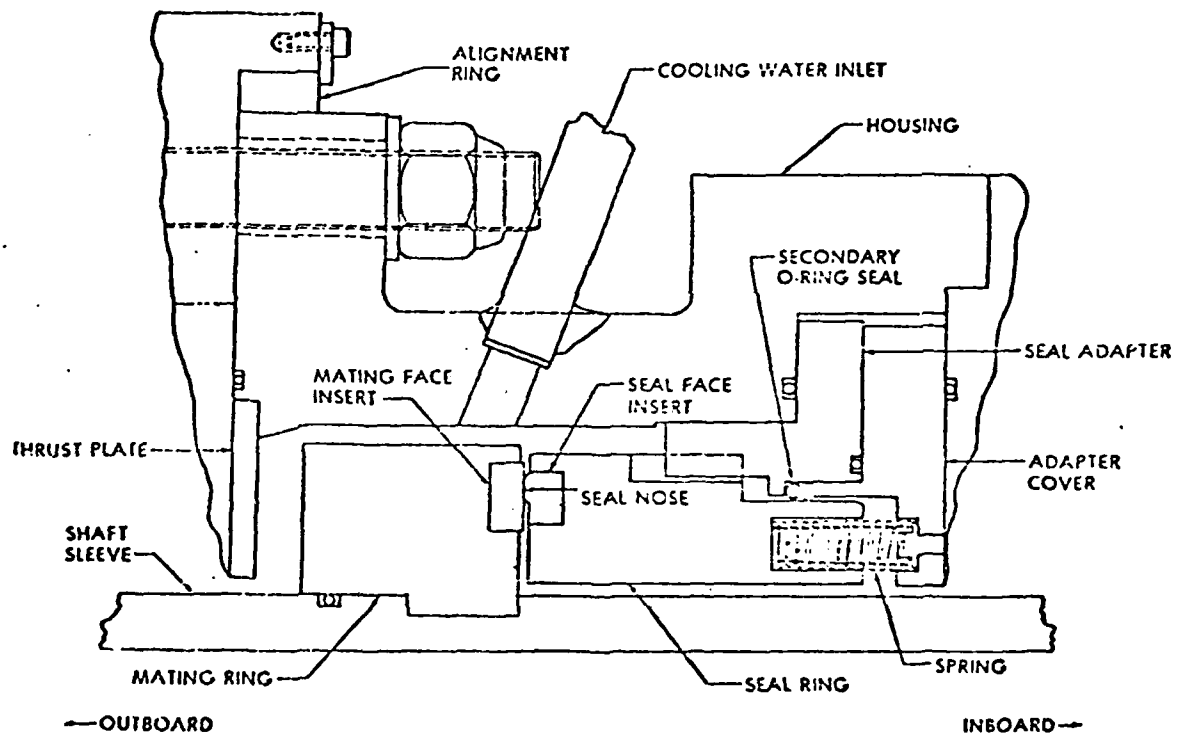
Figure 1. Primary shaft seal assembly.

problems. Figure 2 shows the thermocracked surface of a mating ring from that seal. Numerous radial cracks can be observed on the metallic surface, most of which appear to have originated near the outside of the contact interface. One consequence of the thermocracking shown in Figure 2 was excessive seal leakage, which necessitated replacement of the mating ring.

Thermocracking and its consequences are undesirable in any mechanical face seal, including the shaft seal described here. Unfortunately, attempts to improve face seal designs to avoid thermocracking have often been unsuccessful, primarily because our understanding of thermocracking is very limited. The purpose of this study was to answer several fundamental questions about thermocracking:

-How are thermocracks initiated and propogated?

-How can thermocracks be avoided?

-What material parameters govern conditions leading to crack formation?

-Can the conditions which lead to crack formation be observed in an actual face seal?

The study includes both analytical and experimental efforts whose purpose was to aid in answering these questions.

Previous Studies of Thermocracking

Although thermocracking has been encountered in face seals for many years, it has not been the subject of much intensive study. Much of the work has been experimental in nature and limited in scope. One of the first to discuss the problem was Abar (2), who attributed cracking in ceramic face seal components to thermal gradients caused by frictional heating. He proposed that a ceramic seal ring's resistance to thermocracking can be determined by thermal stress factors used earlier by Kingery (3) in predicting quench cracks in ceramic materials. Later Metcalfe (4) concluded that the cracks are caused by intermittent heating and cooling of the surfaces. He used a thermocrack resistance factor similar to Kingery's.
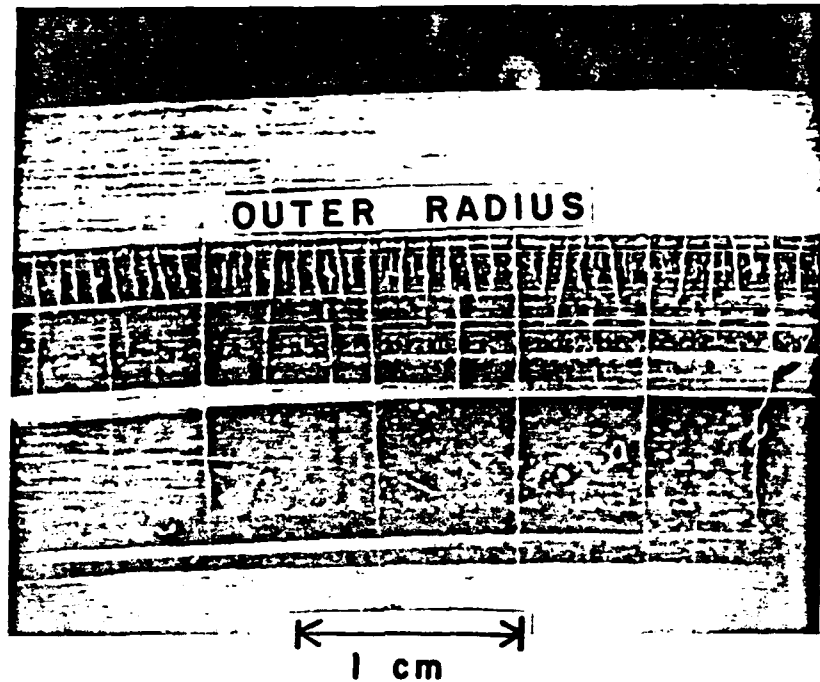
Figure 2.   Photograph of mating ring (insert) surface after seal operation.

The first analytical study of the thermocracking problem was that of Golubiev (5). Although the mechanism of thermocracking was not really established by Golubiev, a criterion for thermocracking, based on excessive thermal stress, was developed. One problem with the Golubiev model is that it assumes that the temperature and stress distributions are both uniform along the sliding interface and does not offer an explanation for the intermittent crack formation apparent in Figure 2. Recent research by Burton and his co-workers (6-8) and by Netzel (9) has shown that frictional heating at the seal interface can become non-uniform at high sliding velocities, with the resulting non-uniform thermal deformation causing contact to become concentrated in a few hot patches on the surface. Temperatures and, presumably, stresses can become quite severe near these hot contact patches, which have come to be called thermoelastic instabilities (TEI). A study of these localized stresses and temperatures must be included in any valid analysis of the thermocracking problems.

MICROSCOPIC OBSERVATIONS OF THERMOCRACKING

In order to get a better understanding of thermocracking in the propeller shaft face seal, an extensive microscopic study of several thermocracked seal rings has been conducted. The complete results of that study were reported elsewhere (10) but will be summarized here.

A radial cross-section of a failed mating ring is shown in Figure 3. The cast cobalt-based material has a coarse grain structure, especially near the top, bottom, and outside surfaces where solidification commenced. Many large second phase particles can be observed, especially near the surfaces. Chemical analysis of these particles shows that they are primarily chromium carbides, with some tungsten carbide also being present. Surrounding the carbide particles is a cobalt-rich solid-solution, face-centered cubic in structure. The seal face, which was originally ground flat, shows substantial wear, with the maximum depth of about .5 mm occurring near the seal inside diameter (region A). Less wear was observed near the outside diameter, where cracks are more prevalent (Region B).

A longitudinal cross-section, cut along a circumferential direction in region B, shows a rather uniform spacing of cracks, all of which appear to be surface-originated (Figure 4). The spacing between cracks can be correlated with the depth of the cracks, with deeper cracks being more widely separated then the shallower cracks. The seal face is not smooth, as can be seen in Figure 4, with substantial surface damage evident in the thermocracked region. Carbon, presumably scraped from the primary seal ring, was present on the surface in the cracked and damaged regions, but was only loosely attached to the mating ring material. A similar slice through region A showed much less surface damage in the region of fewer thermocracks.

A better view of the surface damage is seen in Figure 5, an SEM micrograph of a mating ring surface. Several regions of the surface show evidence of considerable pitting-type damage (regions 1 and 4). This damage is most visible near the seal face outside diameter. Other regions, such as 2, appear to be zones of concentrated contact.
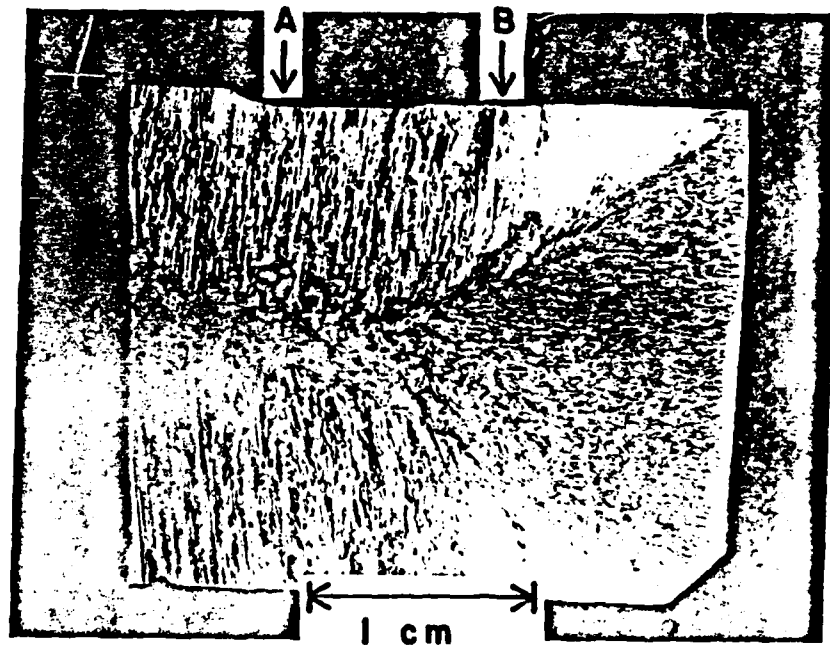
Figure 3. Cross sectional view of mating ring insert after seal operation. Cast cobalt-based superalloy, polished and lightly etched.

100 μm
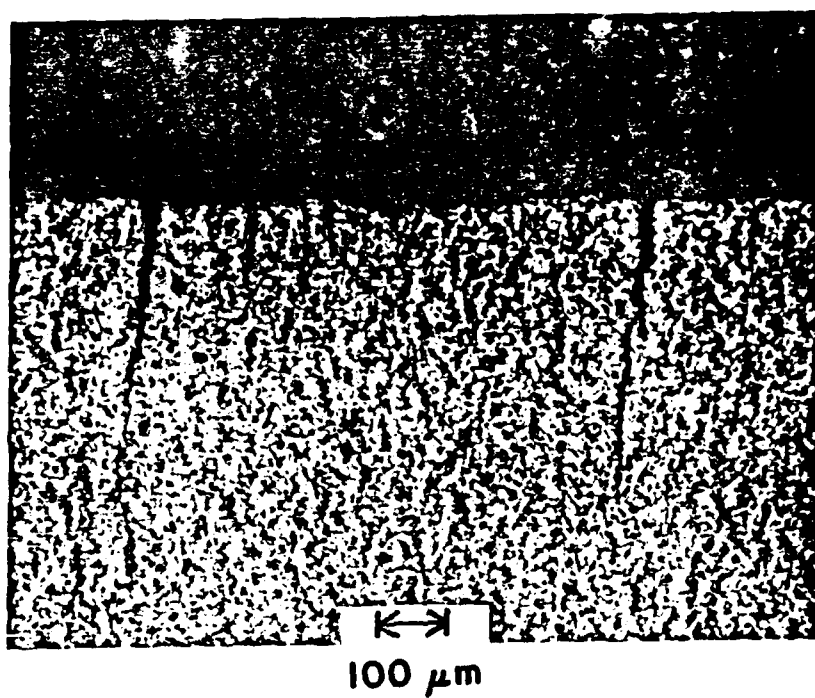
Figure 4. Longitudinal view of mating ring insert after seal operation (sectioned along circumferential direction).
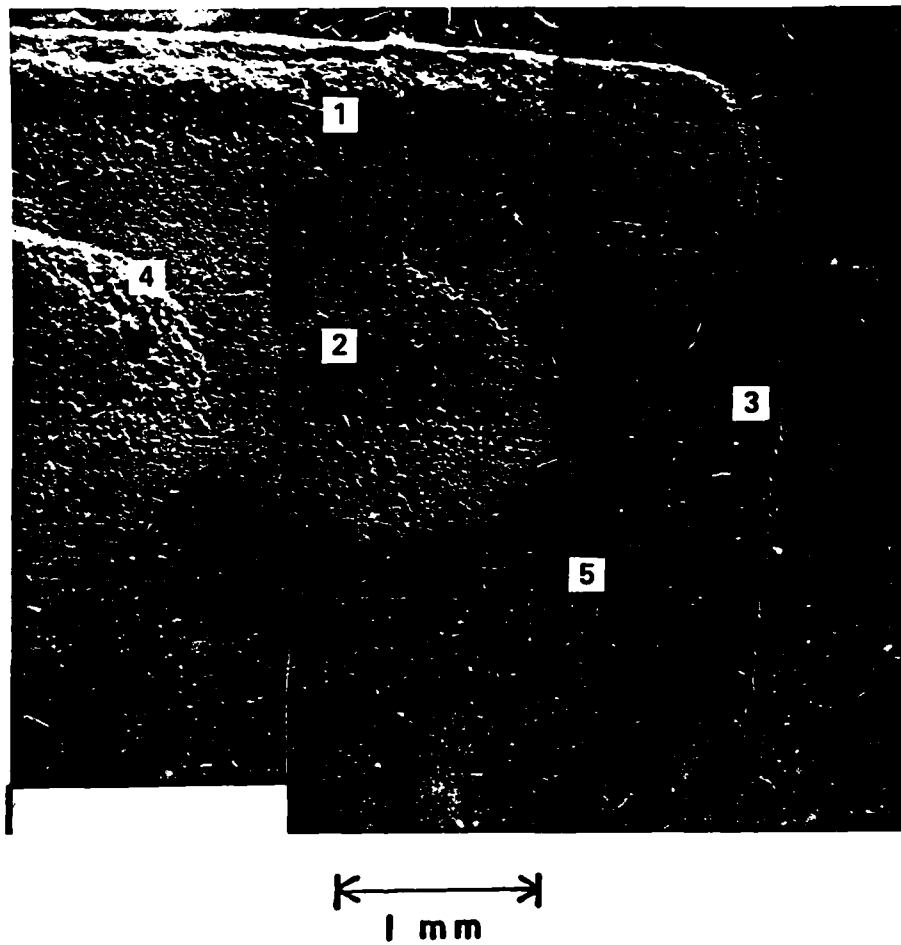
Figure 5. Scanning electron micrograph of mating ring (insert) surface after seal operation.

That contact region includes a crack. Concentrated contact had reoccurred in the region after the crack formed. Region 3 has a large crack, which extends much of the way across the seal face. Other regions, such as 5, especially near the seal inside diameter, appear to be polished, with little evidence of gross damage.

Close examination of the mating ring surface showed several crack initiation sites across the face, with some cracks, such as 3 in Figure 5 , appearing to be formed by a combination of several shorter cracks with different initiation sites. Some of the observed cracks are quite small, either because their growth has been blunted or because the stress was insufficent to cause crack extension. One such microcrack is shown in Figure 6. It was found from Figure 6 and similar micrographs that the cracks tend to begin in the large chromium carbide particles which are visible as dark gray patches. The fracture of the carbides is transgranular in nature, with propagation to other nearby carbides following initiation. If no other carbide particles are close enough, the crack could be blunted in the surrounding ductile cobalt-rich matrix. Another thing evident in Figure 6 is the hole left by removal of a carbide particle. Carbide removal may be responsible for the damage and pitting noted in regions of Figures 4 and 5.

Despite the appearance on the surface of cracks of various lengths, there was no evidence to indicate that they were fatigue cracks. Crack surface appearance was more indicative of brittle fracture produced by rapid unstable crack growth, with fracture of the carbide particles serving as initiation sites.

Although much was learned from these microscopic observations, it is clear that the observations alone do not explain the mechanisms for thermocrack formation and propagation. To complete our understanding of the thermal and mechanical conditions leading to crack formation, an analytical effort was carried out.

Figure 6. Higher magnification SEM micrograph of mating ring (insert) surface after seal operation.

ANALYTICAL APPROACH

The goals of the analytical phase of this work were determination of stress and temperature distributions in the components of the seal shown in Figure 1, and of the material and operating parameters which influence those stresses and temperatures. To accomplish these goals, thermal and thermo-elastic analyses of the contacting seal rings were carried out using finite element methods.

For the purposes of this analysis,it was assumed that thermoelastic instability precedes thermocracking and that contact is concentrated at several (2 or 3) hot patches. Considerable evidence exists, both from our microscopic observations and in recent literature (6-9), to support this assumption. Although our microscopic observations (e.g., Figure 5) suggest that the contact patches are relatively stationary with respect to the rotating mating ring, other investigators have seen hot patches which were stationary on the primary ring and, therefore, moving relative to the mating ring (7,9). Because of this uncertainty, both possibilities were analyzed. An additional uncertainty relates to the number and size of the contact patches. In most of the analyses done here, three identical hot patches were assumed to be located on the seal as shown in Figure 7. The patches were estimated from microscopic observations of the surfaces to be about .1 to 1 mm long and dimensions in this range were used in the study. It was assumed that each of the three contact patches encountered identical conditions, so only one 120^0 sector of the seal needed to be analyzed (see Figure 7). Because of the uncertainty involved in these assumptions, an experimental effort was initiated to determine the size, number, and relative motion of the contact patches in an actual mechanical face seal. That effort is described later in this report.

A finite element model of the shaft seal is shown in Figure 8. The dimensions of the primary seal face insert are shown in Figure 7, with the mating ring insert dimensions being identical except for the thickness, which was slightly larger than that of the primary ring. The finite element mesh was two-dimensional (axial and
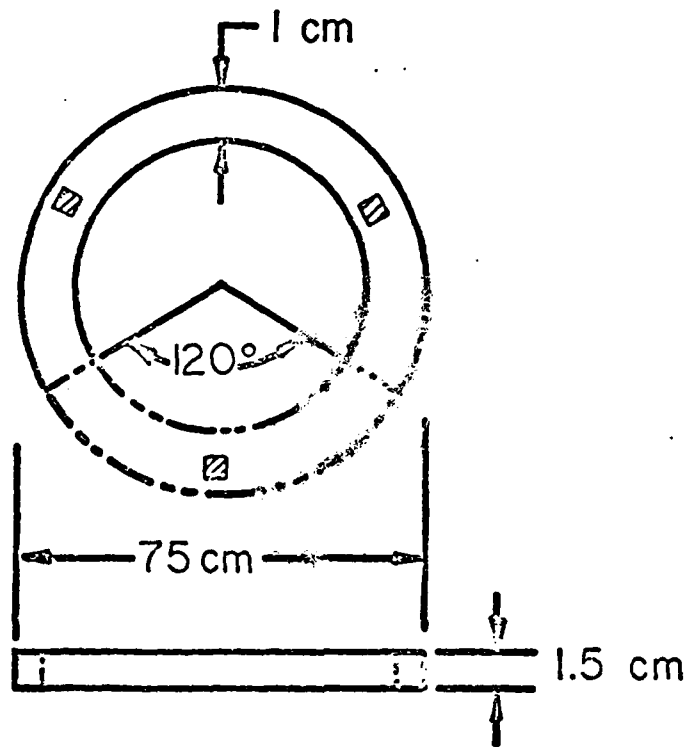
⊠INDICATES ASSUMED CONTACT
  PATCH LOCATIONS
------DESIGNATES PORTION OF SEAL
  COMPONENTS MODELLED IN
  FINITE ELEMENT STUDY

Figure 7. Sketch of primary seal ring, showing section studied in thermal and
stress analyses.
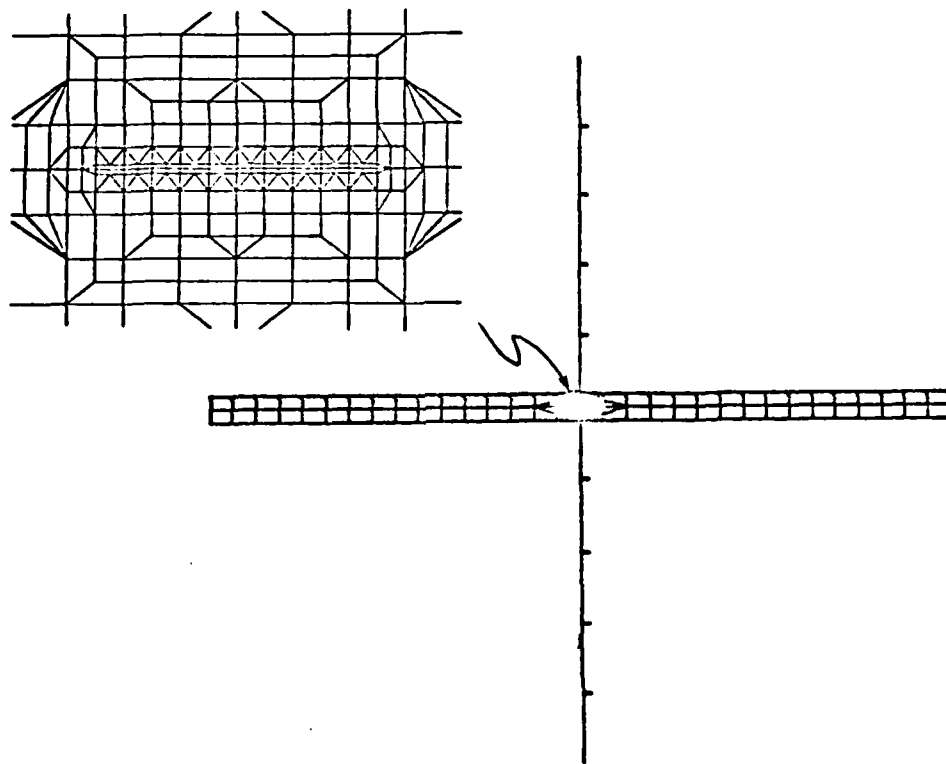
Figure 8. Finite element mesh for shaft seal analysis.

circumferential directions), with variable thickness of the elements being used to account for heat flow in the radial direction. Very fine elements (as small as 10 µm x 30 µm) were used in the contact region, with larger elements being employed further away. A number of different element meshes were tried, with most of the data being generated using a mesh with nearly 700 nodes.

The thermal analysis relied on a finite element program recently developed for studying surface temperatures in sliding systems (11). Before applying the program (THERMAP) to this problem, several modifications of the program were made to expand its capabilities. The accuracy of the program was then tested in a variety of sample problems for which closed-form solutions (12) are available. The program proved to give accurate temperature predictions in both stationary and moving components of a sliding couple, under a wide variety of thermal boundary conditions.

In this case, all frictional heat was assumed to be generated at the nodes within the contact patch. These contact nodes formed a portion of the sealing face of each of the two seal rings, one of which was moving relative to the contact patch, while the other was stationary. Convection boundary conditions were assumed on the non-contacting portions of the seal faces, with fixed temperature boundary conditions being applied on the back sides of each of the seal ring inserts, where they are supported by the large seal and mating rings (Figure 1).

The stress analysis of the seal rings was done using a general purpose finite element thermoelasticity program, FEATS. The temperature distribution calculated in the thermal analysis program was fed into the stress analysis program, along with normal and shear tractions acting at the contact patch. No fluid loading was considered and the supports for the rings were assumed to be rigid. In most cases, only the metallic mating ring was studied in the stress analysis because it was the cracks in that ring that were of most interest here.

Material properties used in most thermal and stress analyses were those of the actual shaft seal ring materials. In one phase of the analytical investigation,

however, the property values were changed to determine the influence of the various material parameters on temperature and stress distributions in the seal rings. The purpose of this parametric study was to provide guidance for material choice for future seal designs.

ANALYTICAL RESULTS AND DISCUSSION

Thermal Analysis

The finite element mesh shown in Figure 8 was used in the thermal analysis of a seal with dimensions shown in Figure 7. Convection to ambient $10^{\circ}C$ water from sides of the seal rings was assumed, with convection coefficients being determined using available heat transfer literature. The back surface of the primary seal ring and the back surface of the mating ring insert (these are the non-rubbing surfaces) were assumed to be held at $10^{\circ}C$. A contact patch of .6 mm length was assumed, based on microscopic observation. The total frictional heat generation rate of 445 W was assumed to be uniformly distributed over the contact patch. A two-dimensional temperature distribution was assumed, with no variation in the radial direction. In many cases it was assumed that convection to sealed fluid occurred at the sealing interface. This interfacial cooling could result from the natural appearance of sealed fluid between the face seals (1) or from the purposeful introduction of fluid at the interface for cooling purposes (9). Netzel (9) has shown that interfacial cooling can diminish the thermocracking problem, and it was desired to find out why this is true.

Analyses of this situation were carried out for two cases: contact patch fixed on stationary primary seal ring, and contact patch fixed on moving mating ring. In both cases the mating ring was assumed to be moving at a velocity of 4.7 m/s and interfacial convective cooling was assumed. Surface temperature distributions for the two cases are shown in Figures 9 and 10. In both cases, as in all other temperature analyses done here, the maximum surface temperature occurs within the contact patch near the trailing edge (the mating ring is moving from left to right in Figure 9 and from right to left in Figure 10). The maximum temperature is more than 40% higher when the contact patch is moving with the mating ring (Figure 10) than when the patch is stationary on the primary ring (Figure 9). This is primarily because the mating

Figure 9. Surface temperature distribution near contact patch in shaft seal. Contact patch stationary with primary ring. Uniform heat generation within patch. Q_{total} = 445 W, Velocity of mating ring = 4.7 ms^{-1}. Interface cooling.
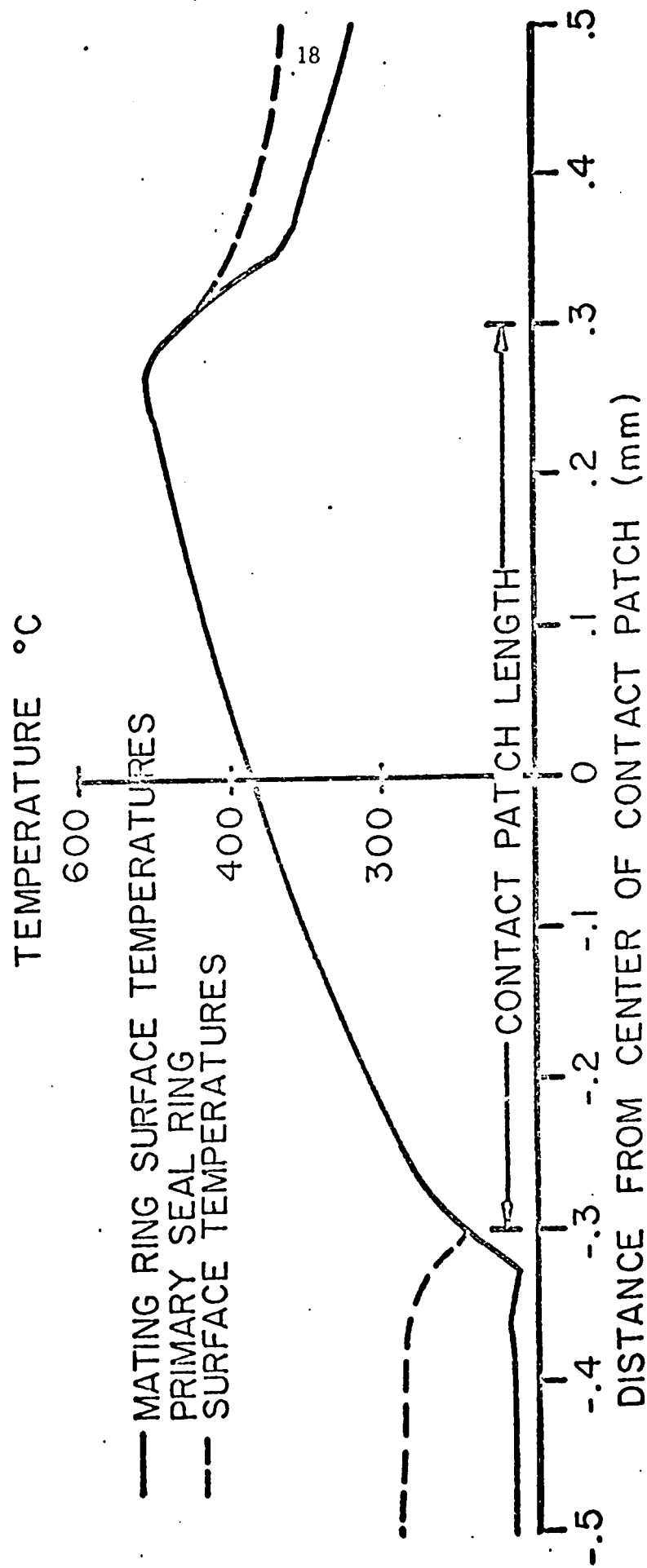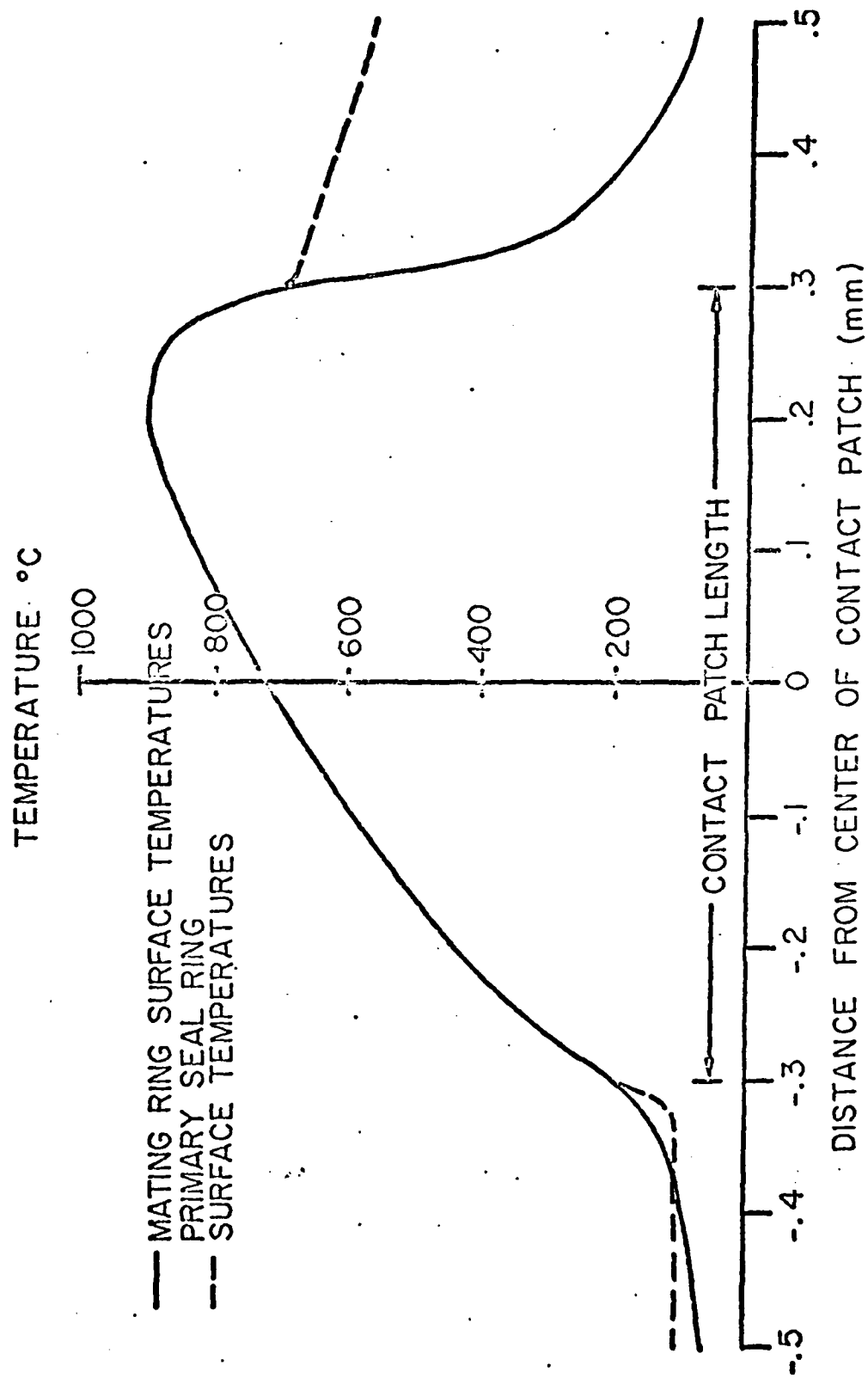
Figure 10. Surface temperature distribution near contact patch in shaft seal. Contact patch moving with mating ring. Uniform heat generation within patch. Q_{total} = 445 W. Velocity of mating ring = 4.7 ms^{-1}. Interface cooling.

ring, which moves with respect to the surrounding water, has a higher convection coefficient acting at its surfaces than acts on the stationary primary ring. The more effective cooling of the mating ring is especially apparent near the leading edge of the contact zone. In both Figures 9 and 10 it can be seen that the mating ring surface tends to be cooler away from the contact patch than does the primary ring. This causes the contact patch temperature to be lower in the case of Figure 9, where the mating ring enters the contact patch and actually cools the primary ring surface.

The high temperatures in the contact patch are very localized, as can be seen from Figure 11, which shows isotherms in both bodies for the same case as was shown in Figure 10. In Figure 11, the mating ring, shown at the top, is moving at a velocity of 4.7 m/s from right to left. The contact patch, which extends from $x = - .03$ cm to $x = + .03$ cm, it is moving with the mating ring. It is evident that temperature gradients in the y direction are larger in the body which is moving relative to the contact patch (in this case the primary ring). One also notes, however, the very severe temperature gradient which occurs on the mating ring surface just to the right of the contact patch. These temperature gradients are important because of their influence on thermal stresses, as will be shown.

Another indication of the relative temperature gradients is shown in Figure 12. Temperatures in the mating ring insert are shown as a function of depth below the center of the contact patch. Comparison is made between three cases: contact patch fixed on moving mating ring, with and without interfacial cooling; and contact patch fixed on stationary primary ring, with interfacial cooling. It can be seen that the most severe axial direction temperature gradients in the mating ring occur in the case when the mating ring is moving with respect to the contact patch, even though the surface temperature magnitudes are lower for that case. The region affected by high temperatures is much larger in the cases where the contact patch is fixed on the mating ring, both because of the higher surface temperatures in that case and

T--MAX = 895.073°C
AT X= 0.018 CM
Y= 0
LABELED WITH 'X'

16 ISOTHERMS
FROM 150° TO 900°C
AT INTERVALS OF 50°

WINDOW
-0.04 TO 0.04 CM
TICK MARKS EVERY 0.008 CM
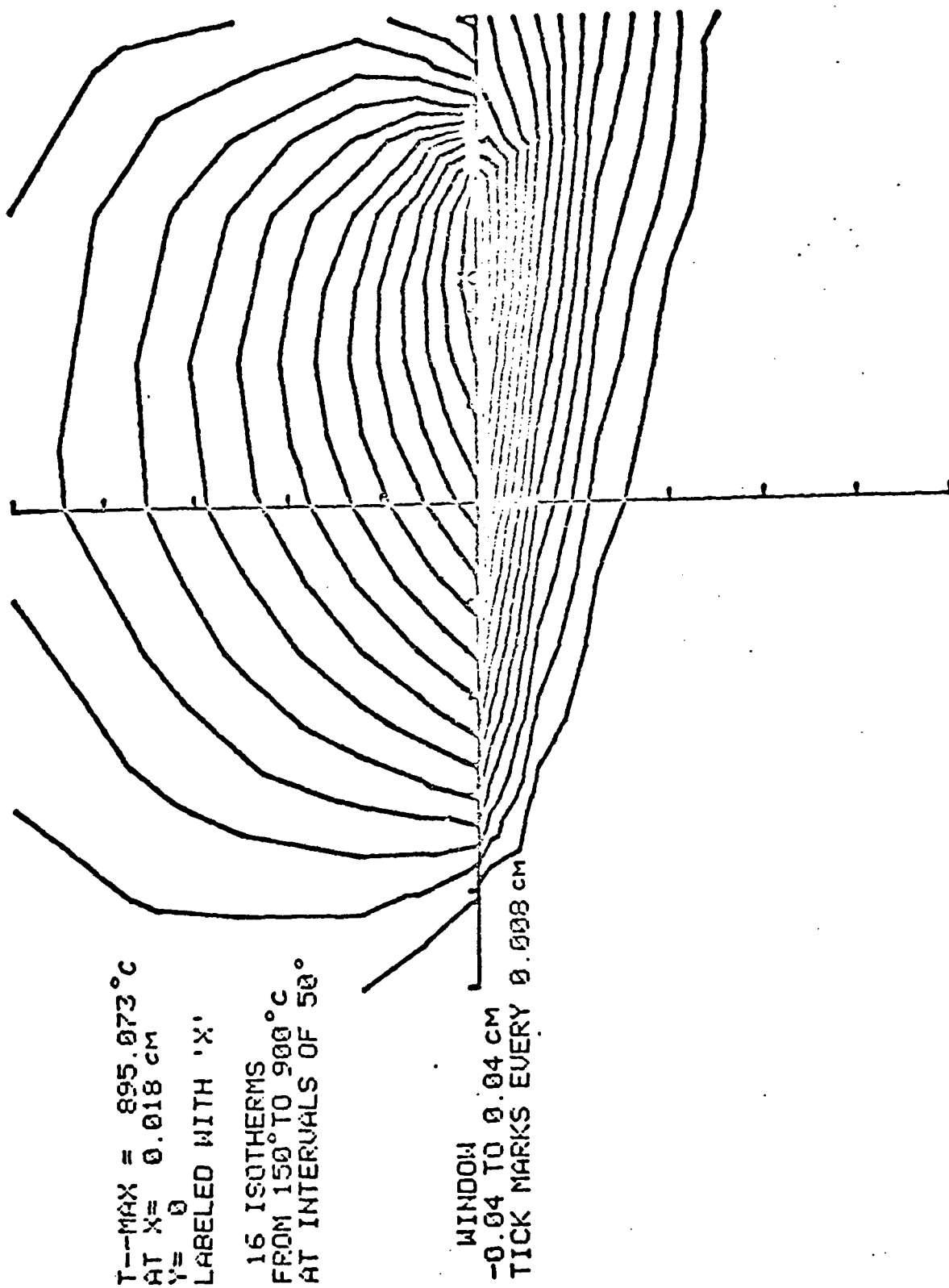
Figure 11. Isotherms in mating and primary rings for case of Figure 10.
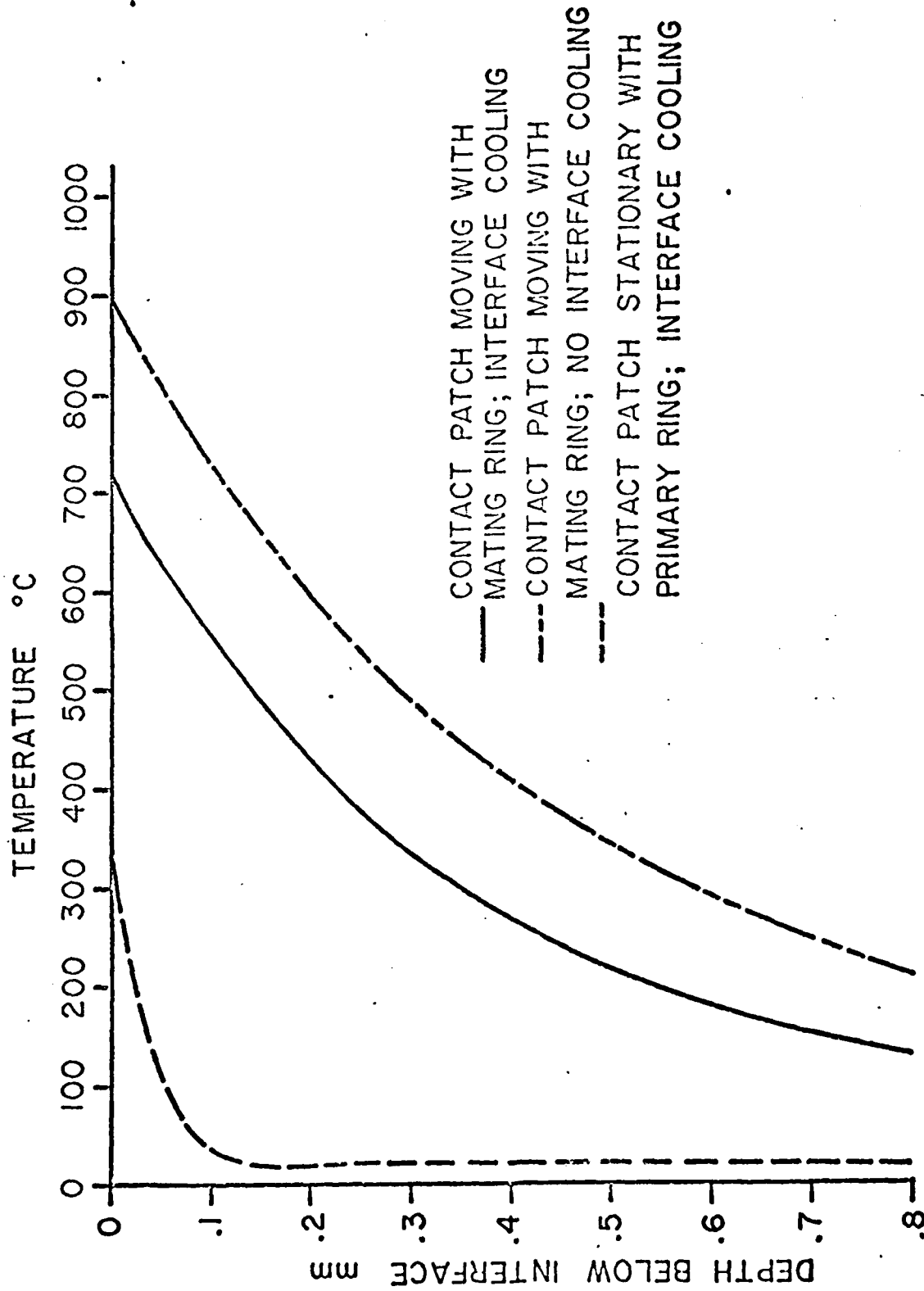
Figure 12. Temperatures within mating ring insert along line through centerline of contact patch. Uniform heat generation within contact patch. Q_{total} = 445 W, Velocity of mating ring = 4.7 ms^{-1}.

Legend within figure:

CONTACT PATCH MOVING WITH MATING RING; INTERFACE COOLING

CONTACT PATCH MOVING WITH MATING RING; NO INTERFACE COOLING

CONTACT PATCH STATIONARY WITH PRIMARY RING; INTERFACE COOLING

TEMPERATURE °C

DEPTH BELOW INTERFACE mm

because of the less severe temperature gradients. Interfacial cooling lowers the temperatures significantly, and also lowers temperature gradients.

Several additional computer runs were carried out to determine the influence on surface tmeperature of heat generation rate Q_{total} and contact length ℓ. It was found, as expected, that an increase in Q_{total} caused a proportional increase in temperatures, all other input variables being equal. A decrease in the length of the contact patch resulted in a small temperature increase in the contact zone, but little or no change at points well-removed from the contact zone. A decrease in patch size from $\ell = .6$ mm to $\ell = .3$mm resulted in an increase of less than 20% in the maximum surface temperature. Therefore, of these two assumed quantities, Q_{total} and ℓ, the thermal analysis is most sensitive to variations in Q_{total}.

Stress Analysis

The stress analysis of the contact region was a plane strain analysis. In most cases only the mating ring material was analyzed. A uniform contact pressure was assumed to be applied to the mating ring by the primary ring in the contact patch region. A uniform shear traction was also assumed to act on the contact patch surface, with the shear traction being equal to the coefficient of friction times the contact pressure. A friction coefficient of 0.5 was used in most analyses. Temperatures calculated in the thermal analysis for a given case were used as input for the thermoelastic stress analysis.

Results of a typical stress analysis are presented in Figure 13. The results are for the case of a contact patch moving with the mating ring, with no interfacial cooling. The normal stress component acting in the circumferential direction, σ_x, is shown, along with the effective stress $\bar{\sigma}$. The effective stress, used in the von Mises yield criterion, is defined in this plain strain case as:

$$\bar{\sigma} = \{\tfrac{1}{2}[(\sigma_x - \sigma_y)^2 + (\sigma_y - \sigma_z)^2 + (\sigma_z - \sigma_x)^2] + 3\tau_{xy}^2\}^{\frac{1}{2}}$$

It can be seen from Figure 13 that σ_x, the stress component which would cause radial cracks like those found in Figure 2, is everywhere compressive. The reason

for this is that the thermal stress, which is compressive, dominates the stress
distribution. The stresses due to surface tractions are tensile in some regions,
particularly at point E, just behind the contact patch. The magnitude of the
contribution to σ_x from tractions alone is very small, however, in comparison
with the contribution from thermal stress. For example, at point E, where σ_x
reaches its maximum value, the contribution from surface tractions is + 33 MPa,
about the same magnitude as the contact pressure acting on the contact patch
(p = 31.7 MPa). The thermal contribution at the same point is -1523 MPa, so it is
by far the dominant factor. In some other situations the difference between thermal
and traction contributions was slightly less, but in all cases the thermal contribu-
tion was dominant and caused the resultant stress distribution to be primarily
compressive.

Some locations in the mating ring were found to have a tensile principal stress
due to the combination of traction and thermal loadings, but their magnitudes were
much smaller than what would be expected to cause fracture. In addition, the orient-
ation and location of those few tensile principal stresses was completely unrelated
to the crack orientations observed in the microscopic examination of seal rings.
Therefore, it was concluded that thermocracking is not caused by tensile stresses
near an active contact patch.

It can be noted from Figure 13 that the effective stress near the contact patch
is quite high. In fact, the effective stress determined in this thermoelastic analysis
is much higher than the yield stress, which is estimated to be about 380 MPa for this
material. It must be concluded, therefore, that significant plastic deformation can
be expected in the region of the contact patch.

The region of high $\bar{\sigma}$, and therefore the region in which plastic deformation
would occur, is concentrated near the contact patch, as can be seen in Figure 14.
By comparing Figure 14 with Figure 12, one can see that the region of high stress is
about the same as the region of high temperature. This is to be expected since the
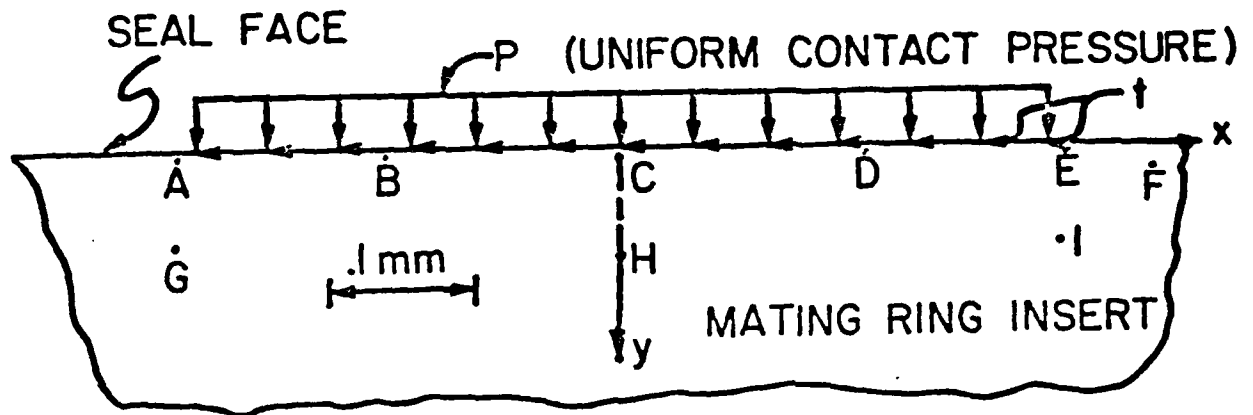
point	T(°C)	σ_x (MPa)	$\bar{\sigma}$ (MPa)
A	337	-1145	1160
B	620	-1250	1242
C	891	-1345	1325
D	1111	-1405	1385
E	1028	-1490	1555
F	753	-1425	1455
G	380	-1140	1160
H	767	-1176	1160
I	843	-1160	1150

Figure 13. Stress distribution within mating ring insert. Conditions same as in Figure 10, except no interface cooling.
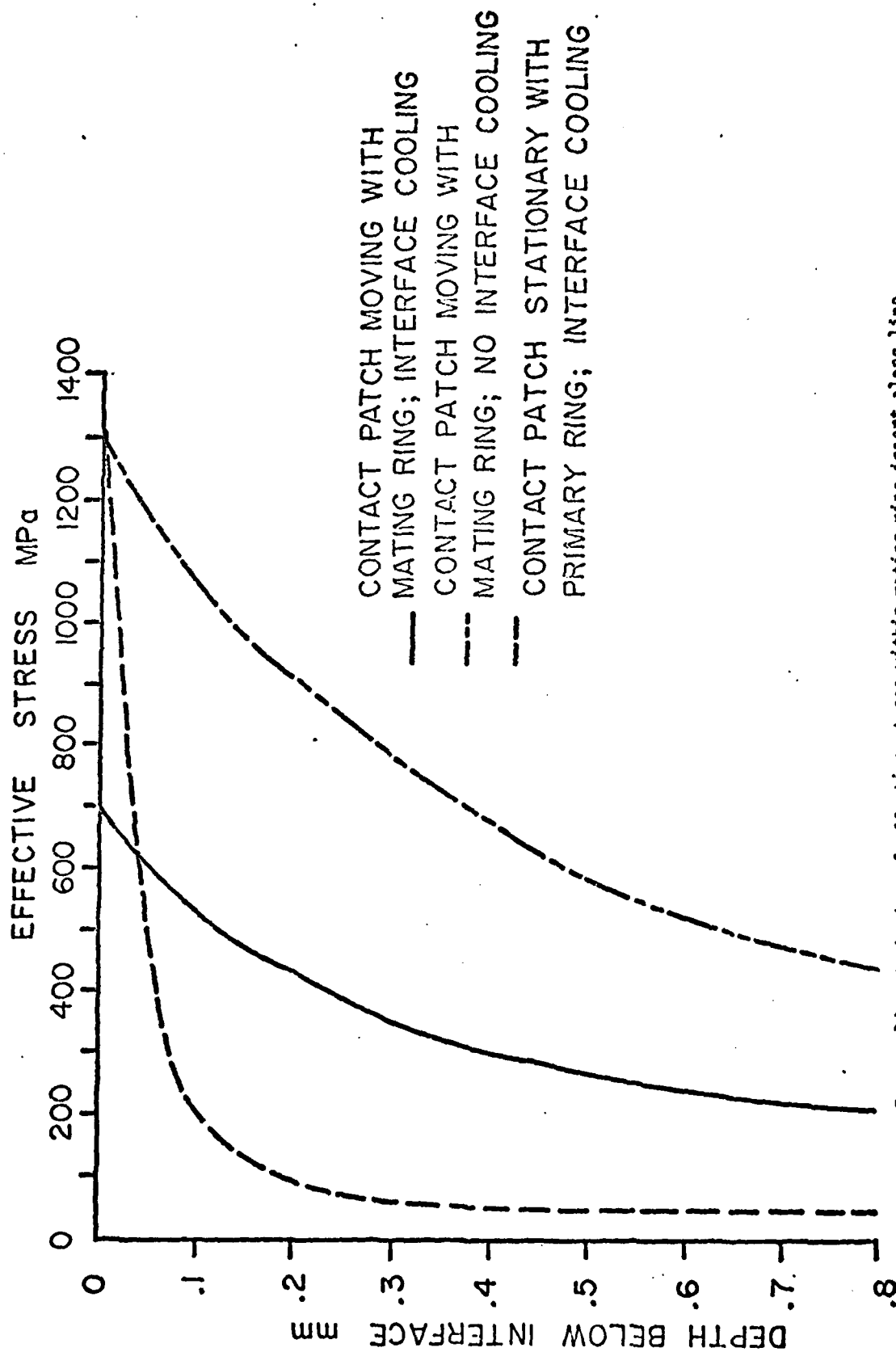
Figure 14. Variation of effective stress within mating ring insert along line. through centerline of contact patch. Q_{total} = 445 W, V = 4.7 ms^{-1}, contact pressure p = 3.17 MPa, shear traction t = .5 p.

dominant contribution to stress is thermal stress. It can also be seen that the lower temperatures found in the situation when the contact patch was fixed on the stationary ring did not guarantee lower stresses in that case. The more severe temperature gradients near the surface in that case led to high stresses (about 85% higher than in the case where the patch was fixed on the moving mating ring). That high stress occurs only very close to the contact surface, however. It can also be seen in Figure 14 that interfacial cooling results in a significant drop in stress levels. This may explain why interfacial cooling has been found to reduce the incidence of thermocracking (9).

CONCLUSIONS FROM ANALYTICAL STUDY

Thermocracking Mechanism

What remains to be established is a connection between ti. predicted plastic deformation in the mating ring near the contact patch and the incidence of thermocracking. It is known that if a localized region is deformed plastically in compression, but is surrounded by a large elastic region, and if the condition causing the plastic deformation is released, then residual stresses are set up in the deformed region which are tensile in nature (see, for example (13)). Essentially, when the plastic deformation in the surrounding material is released, that material wants to return to its original, undeformed, state and in doing so it applied tensile stress to the region which was permanently deformed in compression. If the amount of plastic deformation in the local region is very large, then the tensile residual stresses could be very large also (13). In this seal situation, a large amount of plastic deformation will occur very close to the contact patch. This localized region is surrounded by a large mass of material which remains elastic. If the contact patch now moves elsewhere, the release of the thermal stress will set up residual stress in the region where the patch was located. Since the stress in that region was primarily compressive, with the circumferential stress (σ_x) having by far the largest compressive magnitude, the resulting residual stress will be predominantly tensile, with σ_x being especially large. Thus, a situation is set up whereby tensile cracks (mode I) could be initiated.

In the particular case of the seal examined microscopically earlier in this paper, the cobalt-rich solid-solution surrounding the carbides has a face-centered-cubic structure and plastically deforms quite readily in comparison with the hard carbide particles. The application and then release of a large compressive thermal stress to the material would cause a large residual tensile stress. This tensile stress would act on the hard brittle carbide particles and could cause either fracture of the carbide particle, thus initiating a crack, or breaking of the carbide-matrix

bond, thus allowing the particle to be removed easily. Both forms of damage were observed in Figure 6. If a crack is formed in the region of residual stress, it would tend to relieve the residual strain energy, lowering the residual stress around it. Thus, a contact patch would have to move a good distance away from a crack before buil.ing up a residual stress level sufficient to cause another crack to form. This could account for the spacing between cracks observed in Figures 2 and 3. Thus, the proposed thermocracking mechanism appears to be consistent with all of our microscopic observations.

Alleviation of Thermocracking Problem

Now that a thermocracking mechanism has been established, the avoidance of thermocracks can be addressed. The present mating ring insert material is plagued with two problems: the temperatures, stresses, and residual stresses during seal operation are all quite high; and the presence of many large brittle carbides surrounded by a plastically-deformable matrix leads to easy crack formation in the region of high stress. The easiest way to lessen the chance of thermocracking would be to attack the second problem - reduce the size and enhance the distribution and/or orientation of large brittle carbide particles. It is well known that fracture of aggregates containing brittle second phase particles is mitigated by reducing the size of the particles and the mean free path between them (14). This could possibly be done by a rapid solidification treatment, such as laser or electron beam melting of the surface, or by an improved casting process.

As an alternative, one could attempt to alleviate the cracking problem by choosing a new mating ring material. In such a redesign, it would be desirable to choose a material with properties that would lessen the temperatures and stresses which cause thermocracks. A parametric study was carried out here to determine the influence of various thermal parameters on temperatures and stresses near a contact patch. The results are shown in Table 1. It can be seen that a substantial reduction in both maximum surface temperature and maximum effective stress can be achieved by

TABLE 1

INFLUENCE OF MATERIAL PROPERTIES ON TEMPERATURES
AND STRESSES IN MATING RING

Run #	$\dfrac{k_m}{k_1}$	$\dfrac{k_p}{k_2}$	$\dfrac{\kappa_m}{\kappa_1}$	$\dfrac{\kappa_p}{\kappa_2}$	$\dfrac{E_m}{E_1}$	$\dfrac{\alpha_m}{\alpha_1}$	$T_{max}(^{\circ}C)$	$\bar{\sigma}_{max}(MPa)$
1	1	1	1	1	1	1	895	1050
2	5	1	1	1	1	1	390	460
3	1	5	1	1	1	1	153	240
4	1	1	1	.2	1	1	413	540
5	1	1	1	1	.2	1	895	230
6	1	1	1	1	1	.2	895	230

NOTES:

Subscript 1   refers to properties of cast cobalt-based superalloy.

         2   refers to properties of carbon graphite.

         P   refers to properties of primary seal ring material.

         m   refers to properties of mating ring material.

$k_1 = 1.47 \, k_2$ $\kappa_1 = .6 \, \kappa_2$

All computations are for identical load, velocity, heat input, & cooling conditions. All runs also assume that contact patch rotates with mating ring (moving contact patch relative to primary seal ring). Elastic deformation assumed.

increasing the thermal conductivity (k) of the material which moves with respect to the contact patch. A decrease in the thermal diffusivity (κ) of the same material, or an increase in the conductivity of the opposing material would have a similar, but smaller, effect. Because thermal stress is dominant in this situation, the stress magnitudes are approximately proportional to the product modulus of elasticity (E) and coefficient of thermal expansion (α). Decreases in either of these properties would result in a proportional decrease in stress for a given temperature distribution. Most of the parameters which reduce stresses near a contact patch have also been found to lessen the chance of contact patch formation (8). Choosing a seal material with those properties would be, therefore, especially desirable.

EXPERIMENTAL EFFORT

Experimental Approach

An experimental effort has been underway in conjunction with the analytical effort just described. The goals of the experimental work are twofold: determine the characteristics of the contact patches required for the analytical model (number, size, and location), and verify the analytical predictions of surface temperatures within the hot contact zone. In reference to location, of interest is the specific ring (rotating or stationary) on which the TEI disturbances are formed, and the movement or non-movement of the hot patches on the ring surface. It might be noted that in order to gather this information, none of which has been obtained before for an actual seal, it became necessary to monitor the TEI contact patches during operation of an actual seal, and this had never been successfully reported before.

Because the shaft seal modelled in the analytical investigation was too large to test conveniently, a smaller, commercially-available mechanical face seal was obtained for this test program. The seal consists of a carbon primary ring and a mating ring made of 440 C stainless steel. The sealing surface has a diameter of approximately 5 cm.

In order to determine the presence of TEI-induced contact patches, an electrical contact probe was designed and built. The probe consists of a fine wire implanted in, but insulated from, the stationary seal ring. Figure 15 shows a typical probe loaction in a carbon primary ring, which during initial tests served as the stationary ring. To implant the contact probe a .5 mm diameter hole was drilled in the ring and a .45 mm diameter copper wire, with surrounding epoxy insulation, was embedded in the hole (Figure 16). Against the outer edge of the rotating stainless steel a carbon brush was placed to provide electrical current for the probe. The brush and

brush arm were designed to provide a constant contact pressure in order to avoid spurious signals (Figure 17). The instrument face seal was mounted in a holder on a drill press. The drill press allowed variation of the rotational speed of the rotating ring (8 speeds, ranging from 150 RPM to 1800 RPM), and also allowed control of the contact pressure at the seal interface by means of axial force application. A means of providing pressurized water to the interior of the stationary seal was also provided.

The use of the contact probe to determine the presence of isolated patches of contact at the seal interface is as follows. As thermoelastic instabilities cause separated contact patches to form, contact between the rotating mating ring surface and the embedded wire probe would repeatedly open and close. Since the mating ring material is an excellent conductor, contact between that material and the probe would cause a pulse of direct current to the probe. The resulting signal can be displayed on an oscilloscope.

Problems encountered in the design of the contact probe system centered upon the electrical insulation of both the probe itself and the seal rings, and providing adequate electrical shielding to preserve the integrity of the signal. Early attempts at insulating the rings from the holders failed due to the excessive heat generated at the interface between the seal faces. The problem was resolved by inserting insulating plexiglass discs in the holders at points further removed from the rings to prevent melting (Figures 18 and 19). Sufficient shielding from stray electric and magnetic fields, especially those produced by the drill press motor, were minimized by the use of coaxial cable and grounding of selected parts of the testing apparatus. The complete insulation of the contact probe in the carbon composite can only be partially achieved. Breakdown of the insulation occurs gradually as the surface of the probe begins to wear and loose graphite particles bridge the insulation ring surrounding the wire probe. This causes

CONTACT PROBE

1K

CARBON COMPOSITE RING

SECTIONAL VIEW
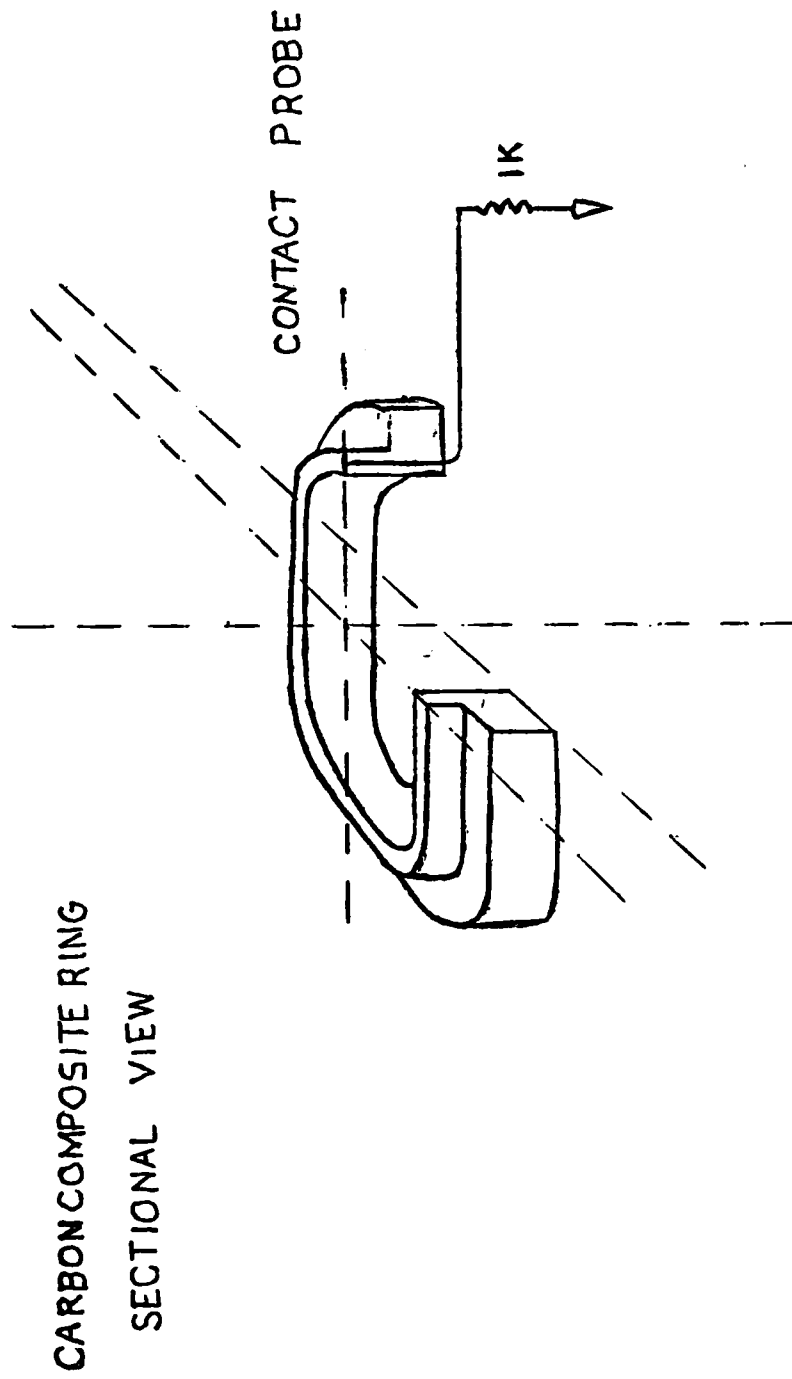
FIGURE 15. Schematic diagram of carbon primary seal ring with embedded contact probe.
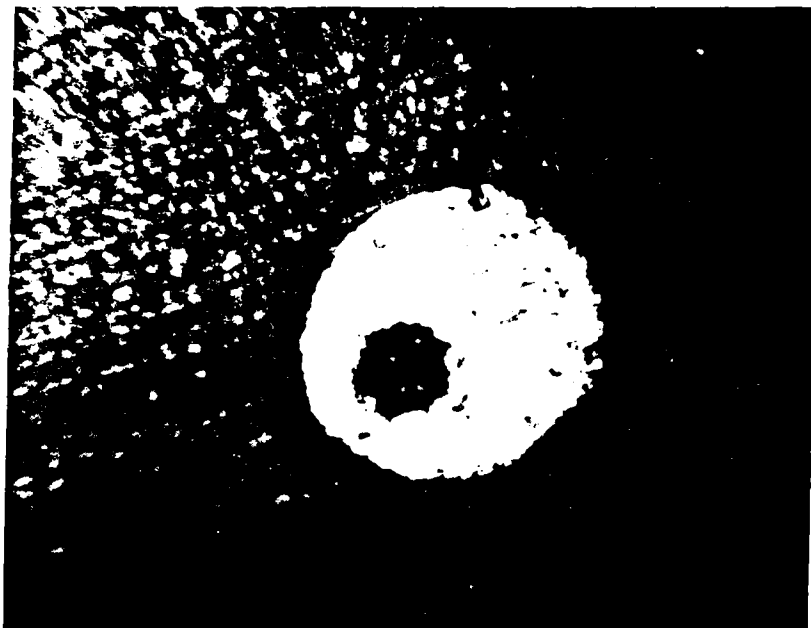
FIGURE 16. Photograph of contact probe wire at contact surface of carbon ring. (100X)

ELECTRICAL BRUSH

GRAPHITE

36

+5 —1K—▷—1M
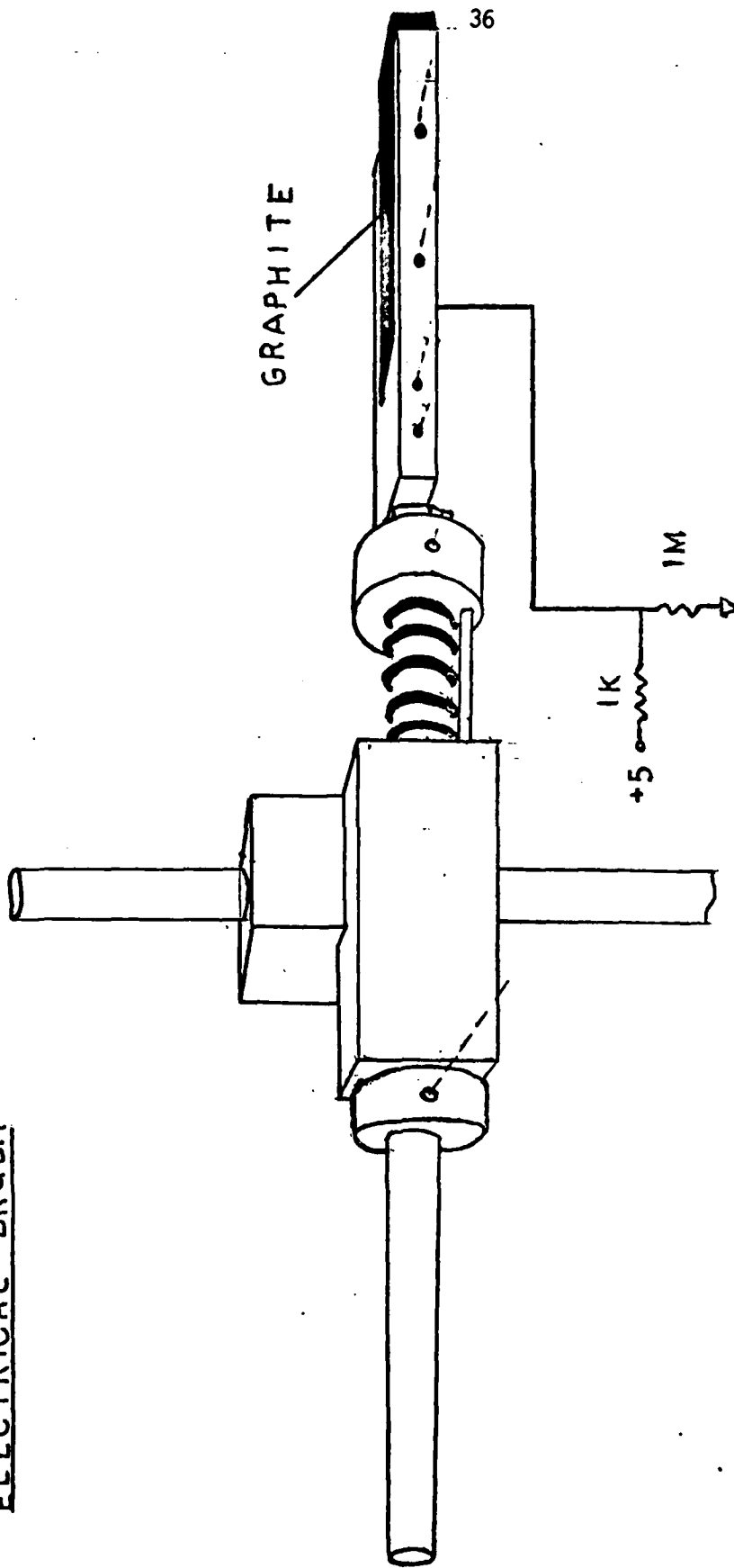
(.2×ACTUAL SIZE)

FIGURE 17.   Schematic diagram of electrical contact brush.

TOP HOLDER

BIT FOR
DRILL
PRESS

PLEXIGLASS
INSULATING
DISC

STAINLESS
STEEL
RING
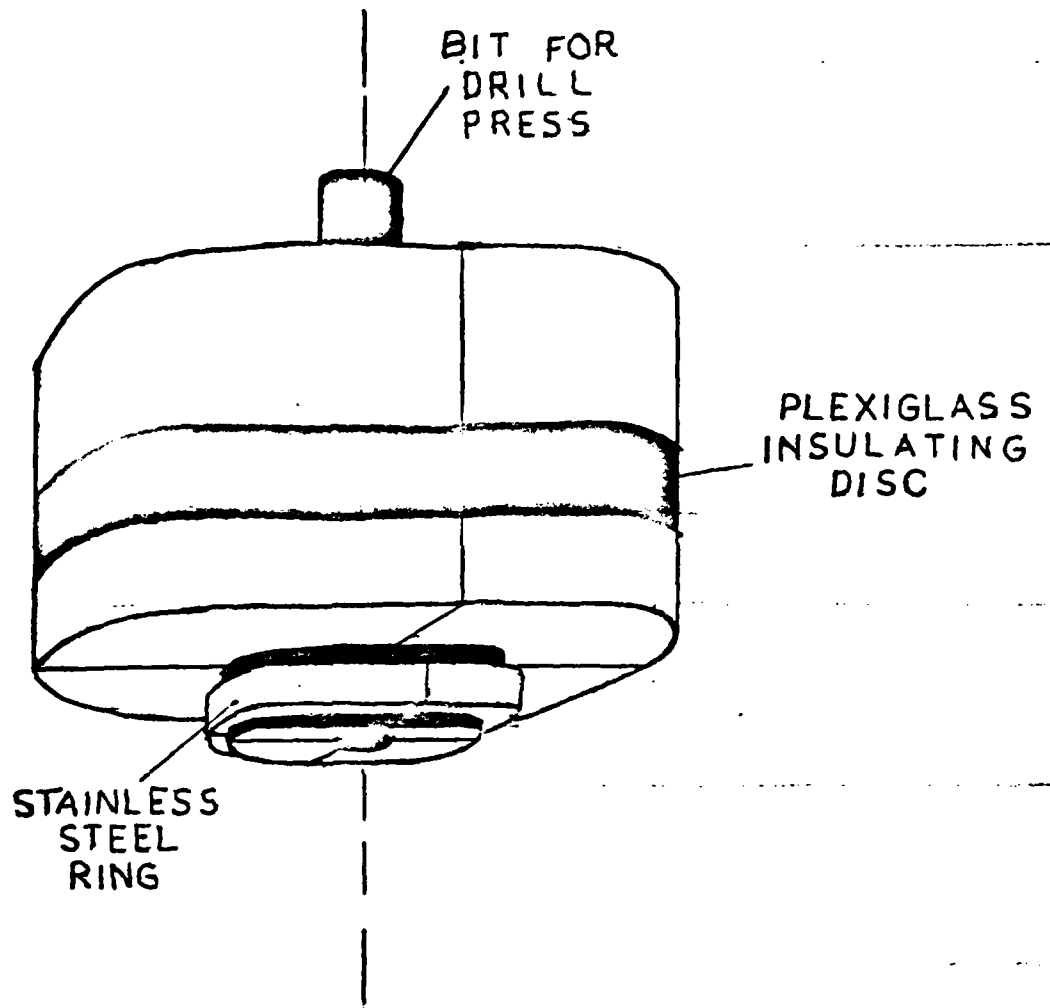
FIGURE 18. Schematic diagram of holder for rotating stainless steel mating ring.

BOTTOM HOLDER

CARBON COMPOSITE RING

INSULATING DISC

MOUNT FOR ELECTRICAL BRUSH

IK

FIGURE 19. Schematic diagram of holder for stationary carbon primary seal ring.

some current to pass from rotating ring to contact probe even when there is
no contact patch at that spot.

To provide a precise measurement of the rotation speed amd more importantly
provide a "location fixed" trigger source, a tachometer employing a photon
coupled interrupter has been designed and is under construction. The purpose
of a location fixed trigger source is to determine whether the contact patches
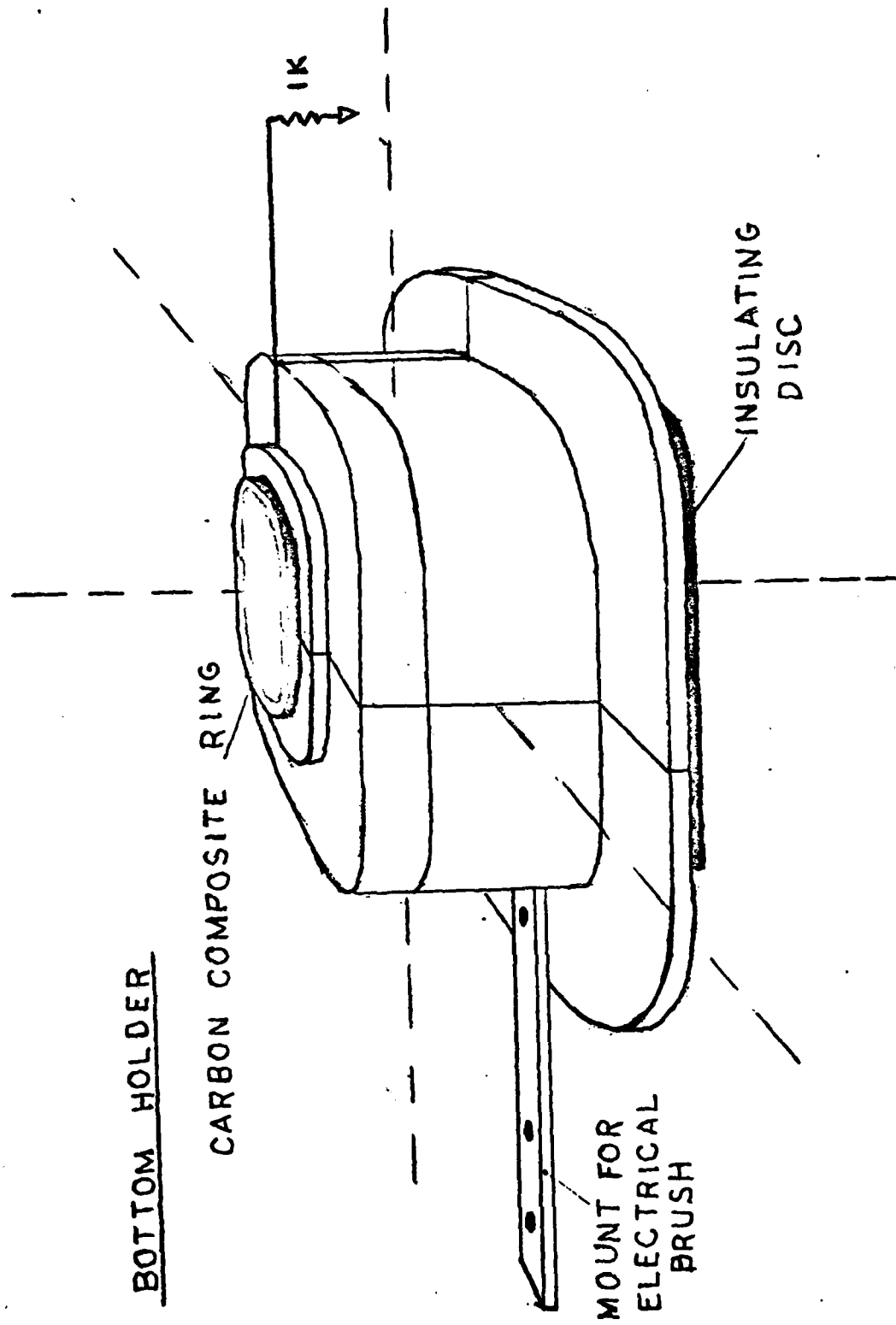are stationary or in slow rotation on the ring surface.

Considerations for the technique to employ for instantaneous temperature
measurement of contact patches center upon the use of a dynamic thermocouple. The
thermocouple junction will be formed by the rotating stainless steel ring, an iron
based alloy, and a metallic probe of constantan embedded in a manner similar to the
placement of the electric contact probe. The junction voltage difference will then
be displayed on an oscilloscope screen. The usefullness of such a dynamic thermo-
couple in measuring surface temperatures in sliding contacts has been proven in
other recent work in our laboratory (15). The probe for this project is still under
development, however.

With the objective of providing a coherent method of data collection, a
three-channelled digital storage oscilloscope has been designed. Employing an
Intel 8088 CPU, the storage oscilloscope can selectively change the sampling rate
and trigger level. The final stages of software development are near completion.
The storage oscilloscope will be used to display simultaneously the size of each
contact patch, the corresponding junction voltage drop, i.e. temperature, and the
relative location of each patch with respect to the fixed position pulse of the
tachometer.

Preliminary Experimental Results

Initial experimentation with the contact probe has verified the presence of
TEI-induced contact patches on the surface of the 440C stainless steel mating ring.
A typical trace of current from the contact probe is shown in Figure 20. Contact
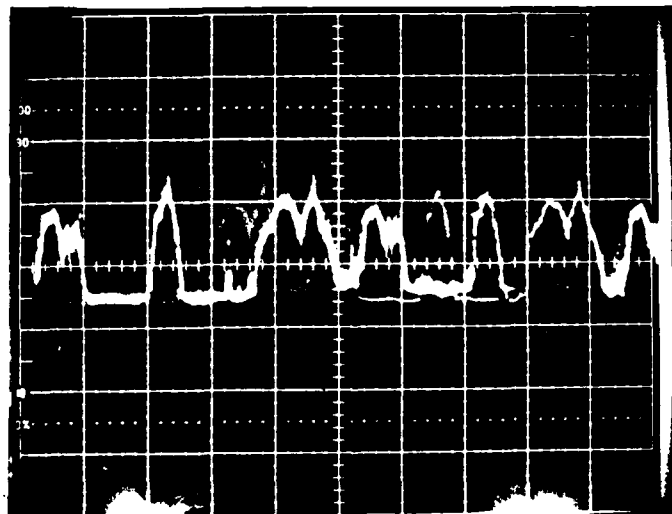
FIGURE 20. Contact probe output at 20 rev/sec, early during test (horizontal scale: 10 msec/div, vertical scale: 2 V/div).

between the moving ring and the stationary probe wire is indicated by voltage peaks. The test was run dry at a speed of 20 rev/sec (or 50 msec/rev). It can be seen that three contact patches or bumps are present on the mating ring surface and seem to be rotating with it. The patches do not appear to be identical, with one of them extending over about one-fourth of the ring surface. The problem mentioned earlier concerning current leakage from carbon ring to contact probe wire is demonstrated in Figure 21. The signals from the contact patches themselves remain unaltered while the voltage level of the non-contacting region continually rises.

The influence of velocity on thermoelastic instabilities is shown in Figure 22. That trace was taken from a test run at 30 rev/sec (33 sec/rev), with all other conditions being the same as in test of Figures 20 and 21. It can be seen that there are still three contact patches on the mating ring surface and rotating with that ring. The patches appear to be sharper (smaller) than those in the slower tests.

Up to now the experimental efforts have focused on developing the techniques for studying TEI phenomena in mechanical face seals. Having verified the existence of TEI-induced contact patches, further testing is now underway to study the influence of various operating and geometric factors on the formation of these patches. Use of the recently-developed instrumentation to enable quantification of the information about contact patches is also proceeding. This information will be used in the analytical model described earlier. The next step in the experimental work will be the use of the dynamic thermocouple in the measurement of surface temperatures within the contact patches.
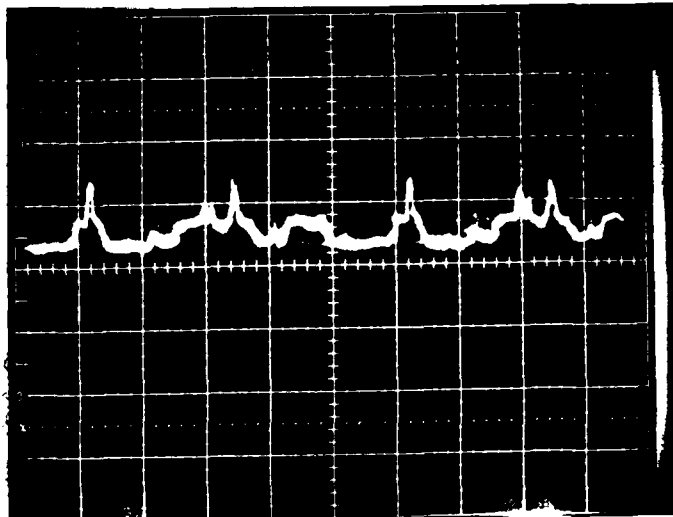
FIGURE 21. Contact probe output at 20 rev/sec, later in test. (horizontal scale: 10 msec/div, vertical scale: 2 V/div).
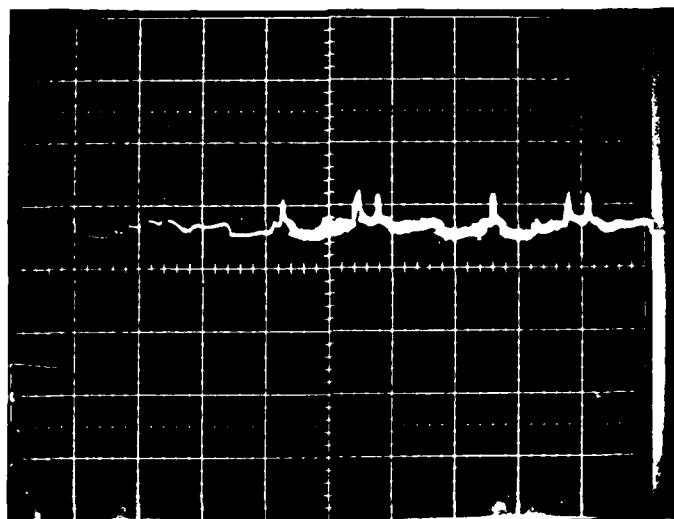
FIGURE 22. Contact probe output at 30 rev/sec, (horizontal scale: 10 msec/div, vertical scale: 2 V/div).

SUMMARY

Microscopic Observations

Examination of the worn and cracked surface of a cobalt-based mating ring of a large marine shaft seal revealed that thermocracks are initiated by cracking of large brittle chromium carbides found on the surface of the cast mating ring material. Some of the carbides were plucked out and these appeared to cause surface damage.

Experimental Study

An electrical contact probe has been developed which enables determination of the presence of thermoelastic instability-induced patches of contact on the surface of a mechanical face seal. The probe showed that these localized contacts do occur on the seal ring interface and that an increase in sliding speed tends to cause a sharpening or concentration of the contact patches. Work is continuing on this study in an attempt to determine the size, number, and location of the contact patches and the surface temperature within them.

Analytical Model

A finite element-based computer model has been developed which enables the determination of temperature and stress distributions near the concentrated contact patches. The analytical model assumes that thermoelastic instabilities at the sealing interface led to the formation of the contact patches prior to the onset of thermocracking. The analysis showed that high temperatures and resulting thermal stresses can occur in the mating ring whether the contact patches be stationary relative to the moving mating ring or relative to the stationary primary sealing ring. Although the thermal stresses are compressive, the release of the thermal stresses caused by movement of the contact patch results in a residual tensile stress on the surface. The action of these residual stresses on the carbide particles

appears to be responsible for the onset of thermocracking.

The incidence of thermocracking could be reduced by either reducing the size and controlling the shape and distribution of carbide particles or by choosing a new material with properties that would lead to smaller temperatures and stresses near the contact patches. If the later course of action were followed, it would be desirable to choose a seal material with low modulus of elasticity, low coefficient of thermal expansion, high thermal conductivity, and high fracture strength. One must bear in mind, however, the fact that many of the material properties and microstructural characteristics which influence thermocracking also affect other modes of seal failure such as wear. Material choices should be made which alleviate the thermocracking problem without increasing wear.

REFERENCES

1. L.P. Ludwig and H.F. Greiner, "Designing Mechanical Face Seals for Improved Performance," Mechanical Engineering, Nov. 1978, 38-46.

2. J.W. Abar, "Rubbing Contact Materials for Face Type Mechanical Seals," Lubrication Engineering, V.20 (1964), 381-386.

3. W.D. Kingery, "Factors Affecting Thermal Stress Resistance of Ceramic Materials," J. American Ceramic Soc., V.38 (1955), 3-15.

4. R. Metcalfe, "End Face Seals in High Pressure Water - Learning from the Failures," Lubrication Engineering, V.32 (1976), 625-636.

5. A.I. Golubiev, "Thermocracking of Seal Faces in Mechanical Seals," Proc. 5th Int. Conf. on Fluid Sealing, Warwick, England, 1971, A2-9 to A2-16.

6. R.A. Burton, V. Nerlikar, and S.R. Kilparti, "Thermo-Elastic Instability in a Seal-Like Configuration," Wear, V.24 (1973), 177-188.

7. B.N. Banerjee and R.A. Burton, "Experimental Studies of Thermoelastic Effects in Hydrodynamically Lubricated Face Seals", Trans. ASME, J. Lubrication Technology, v. 101 (1979), 275-282.

8. R.A. Burton, "Thermal Deformation in Frictionally Heated Contact," Wear, v. 59 (1980), 1-20.

9. J.P. Netzel, "Surface Disturbances in Mechanical Face Seals from Thermoelastic Instability," Lubrication Engineering, v. 37 (1981), 272-278.

10. S.A. Karpe, V.A. Surprenant, and R.G. Brown, "Surface Deterioration in a Seal Mating Ring Insert," presented at Navy/NASA Liquid Lubricated Seal Workshop, Alburquerque, NM, October 1981.

11. F.E. Kennedy, "Surface Temperatures in Sliding Systems - A Finite Element Analysis," Trans. ASME, J. Lubri :tion Technology, v. 103 (1981), 90-96.

12. H.S. Carslaw and J.C. Jaeger, "Conduction of Heat in Solids," 2nd ed., Oxford Univ. Press, London, 1959.

13. F.E. Kennedy and F.F. Ling, "Elasto-Plastic Indentation of a Layered Medium," Trans. ASME, J. of Engineering Materials and Technology, v. 96 (1974), 97-103.

14. A.S. Tetelman and A.J. McEvily, Jr., Fracture of Structural Materials, John Wiley and Sons, Inc., New York (1967), p. 659.

15. F.E. Kennedy, "Single Pass Rub Phenomena - Analysis and Experiment", to be published in ASME Journal of Lubrication Technology, ASME Preprint ≠81-Lub-55.

Distribution List

Recipient	Number of Copies
Office of Naval Research 800 N. Quincy Street Arlington, Virginia 22217 Attn: M. Keith Ellingsworth, Code 473	(3)
Defense Documentation Center Building 5 Cameron Station Alexandria, Virginia 22314	(12)
Naval Research Laboratory 4555 Overlook Avenue Washington, DC 20390 Attn: Technical Information Division 　　Code 2627 　　Dr. Ravner, Code 6170	 (6) (1)
U.S. Naval Postgraduate School Monterey, California 93940 Attn: Dept. of Mechanical Engineering	(1)
U.S. Naval Academy Annapolis, Maryland 21402 Attn: Dept. of Mechanical Engineering	(1)
Naval Air Systems Command Jefferson Plaza Washington, DC 20360 Attn: B. Poppert, Code 240E	(1)
Naval Air Systems Command Crystal City, National Center #3 Washington, DC 20360 Attn: Frank Ventriglio, Code OSR14	(1)
Naval Ships R&D Center Annapolis, Maryland 21402 Attn: Friction and Wear Branch 　　J.F. Dray	(1)
Naval Air Engineering Center Lakehurst, New Jersey 08733 Attn: Mr. P. Senholzi	(1)
Naval Air Propulsion Test Center Trenton, New Jersey 08628 Attn: Mr. R. Valori	(1)

Distribution List (continued)

Recipient	Number of Copies
Naval Air Development Center Warminster, Pennsylvania 18974 Attn: Mr. A. Conte	(1)
National Science Foundation 1800 G Street, NW Washington, DC 20550 Attn: Dr. C.J. Astill	(1)
National Bureau of Standards Washington, DC 20234 Attn: Dr. W. Ruff	(1)
NASA Lewis Research Center 21000 Brookpark Road Cleveland, Ohio 44135 Attn: L.J. Kiraly	(1)
Air Force Office of Scientific Research Washington, DC 20333 Attn: Directorate of Engineering Sciences	(1)
Air Force Aeropropulsion Laboratory Wright-Patterson Air Force Base, Ohio 45433 Attn: AFAPL/POD-1, Dick Quigley, Jr.	(1)
Army Research Office Durham, North Carolina 27706 Attn: Dr. E.A. Saibel	(1)
Office of Naval Research Branch Office 1030 East Green Street Pasadena, California 91106	(1)
Assistant Chief for Technology Office of Naval Research, Code 200 Arlington, Virginia	(1)
Prof. H.S. Cheng Department of Mechanical Engineering Northwestern University Evanston, Illinois	(1)
Crane Packing Company 6400 Oakton Street Morton Grove, Illinois 60053 Attn: Art Zobens	(1)

Distribution List - continued

Recipient	Number of Copies
Sealol, Inc. Box 2158 Providence, Rhode Island 02905 Attn: H.F. Greiner	(1)
Pure Carbon Company St. Marys, Pennsylvania 15857 Attn: R.R. Paxton	(1)
Franklin Research Institute 20th and Race Streets Philadelphia, Pennsylvania 19103 Attn: Harry C. Rippel	(1)
Naval Sea Systems Command Crystal City, National Center #3 Washington, DC 20360 Attn: Code 524, Dick Graham	(1)
Naval Ships R&D Center Annapolis, Maryland 21402 Attn: Al Harbaugh	(1)
Profs. A.O. Lebeck and F.D. Ju Dept. of Mechanical Engineering University of New Mexico Albequerque, N.M. 81731	(2)
Mr. Cliff Mussen PMS 396-223 Trident Submarine Ship Acquisition Project Naval Sea Systems Command Department of Navy Washington, DC 20362	(1)
Prof. Ralph Burton Dept. of Mechanical Engineering North Carolina State Univ. Raleigh, North Carolina 27650	(1)

3 — 8

DTIC